Published online 16 June 2020

Nucleic Acids Research, 2020, Vol. 48, No. 15 ***e89***
doi: 10.1093/nar/gkaa521

High-throughput methods for measuring DNA thermodynamics

Jin H. Bae [1], John Z. Fang[1] and David Yu Zhang [1,2,*]

[1]Department of Bioengineering, Rice University, Houston, TX, USA and [2]Systems, Synthetic, and Physical Biology, Rice University, Houston, TX, USA

Received November 28, 2019; Revised May 25, 2020; Editorial Decision June 06, 2020; Accepted June 08, 2020

ABSTRACT

Understanding the thermodynamics of DNA motifs is important for prediction and design of probes and primers, but melt curve analyses are low-throughput and produce inaccurate results for motifs such as bulges and mismatches. Here, we developed a new, accurate and high-throughput method for measuring DNA motif thermodynamics called TEEM (Toehold Exchange Energy Measurement). It is a refined framework of comparing two toehold exchange reactions, which are competitive strand displacement between oligonucleotides. In a single experiment, TEEM can measure over 1000 ΔG° values with standard error of roughly 0.05 kcal/mol.

INTRODUCTION

DNA and RNA molecules fold via Watson–Crick interactions to form secondary structures, which are important both biologically and biotechnologically in determining reaction accessibility (e.g. regulation by microRNAs (1); kinetics of PCR amplification or hybrid-capture (2)). Algorithms that predict nucleic acid folding and structure (3,4) inherently rely on a thermodynamics model (5–8) to rank the many potential structures against one another. Because there exist exponentially many DNA sequences of a particular length, it is not feasible to comprehensively characterize the thermodynamics of all sequences. Instead, the commonly accepted nearest neighbor (NN) model (9) considers the standard free energy of formation ΔG° of a DNA structure to be the sum of ΔG° values for non-overlapping independent motifs such as base pair stacks (Figure 1A).

The NN model has been experimentally shown to be quite accurate for complementary DNA strands that form perfect duplexes (10). However, biological DNA sequences frequently contain destabilized duplexes with mismatches or bulges, for example through enzymatic misincorporation during replication (11,12) or environment-induced oxidation and deamination (13,14). Furthermore, oligonucleotide primers and probes used for molecular biology and genomics, when bound to variant genomic DNA sequences, form imperfect duplexes. Understanding the thermodynamics of these destabilizing motifs is thus important for both understanding the behavior of biological DNA molecules, and to guide the design of oligonucleotide reagents.

In our studies of the thermodynamics of single-base DNA bulges using high-resolution melt (HRM) (15), we found that four different DNA duplexes bearing the same single-base bulge motif yielded very different motif-specific thermodynamic penalty ($\Delta\Delta G^\circ$) values (Figure 1B and C). This result implies that the melt curve analysis methods with which many DNA motif thermodynamic parameters are measured are inaccurate. Table 1 summarizes major limitations of conventional methods such as HRM, UV melting, isothermal titration calorimetry (ITC), and differential scanning calorimetry (DSC). The major drawback of these methods is that the temperature range over which ΔG° can be accurately inferred is limited. Because temperature range of the fitting is limited by a series of melting temperatures (T_m) (or any single temperature for ITC), the thermodynamic parameters can deviate significantly with extrapolation to temperatures outside the T_m range. This problem is exacerbated by the fact that motif $\Delta\Delta G^\circ$ is computed by numerically subtracting ΔG° of a reference (stable duplex with only canonical base pairs) vs. bulge duplex but the two duplexes' T_m ranges may have little to no overlap.

To investigate the inconsistent HRM results, we developed a new method called Toehold Exchange Energy Measurement (TEEM) to independently measure the thermodynamics of bulges and other DNA motifs. TEEM continuously measures ΔG° of a motif at multiple temperatures by using toehold exchange reaction (16) instead of heating DNA. Conventional methods infer (spectroscopic methods) or measure (calorimetric methods) a single pair of ΔH° and ΔS° from each experiment, which are extrapolated to provide ΔG° values. TEEM, on the other hand, generates an independent ΔG° value at each temperature point across a wide range of temperatures. As a result, the number of ΔG° values measured per experiment is at least 40 times more than those by other methods. The strongest advantage of TEEM is that it can discover subtle trends in

*To whom correspondence should be addressed. Tel: +1 626 390 2242; Email: dyz1@rice.edu

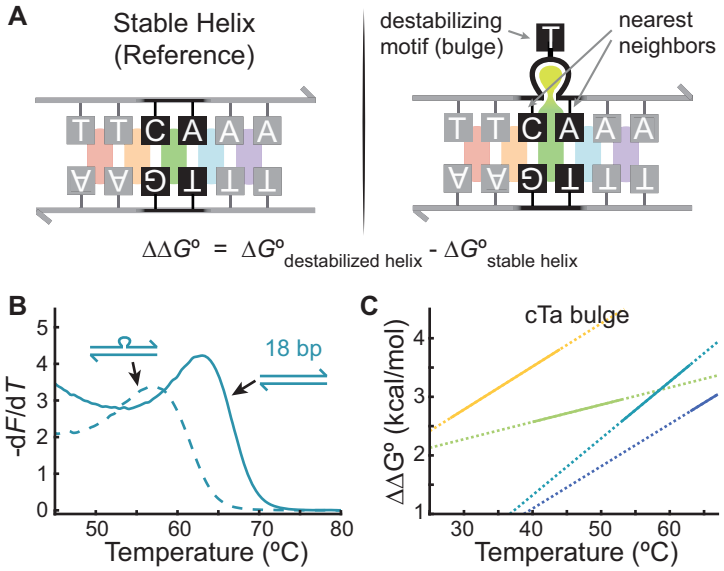

Figure 1. Thermodynamics of DNA duplex destabilization. (**A**) The nearest neighbor (NN) model of DNA hybridization considers the standard free energy of formation of a DNA molecule (ΔG°) to be the sum of the ΔG° of individual motifs, such as base pair stacks. Destabilization of the motif, such as via a single-base insertion that results in a bulge in the right panel, introduces a motif-specific thermodynamic penalty ($\Delta\Delta G^\circ$). (**B**) High-resolution melt (HRM) analysis of a 18 bp duplex (solid line) and a 18 bp duplex with a single base bulge (dotted line). From these data, the standard enthalpy (ΔH°) and standard entropy (ΔS°) of the two molecules can be fitted, and numerical subtraction generates $\Delta\Delta H^\circ$ and $\Delta\Delta S^\circ$ values for the bulge motif. (**C**) We performed HRM analysis on four different pairs of DNA duplexes of different lengths, in order to measure the $\Delta\Delta G^\circ$ of a single nucleotide T bulge, flanked by a C and an A to the 5′ and 3′ ends (cTa bulge). Here, the HRM-measured ΔG° values are separated into high-confidence ranges (solid lines) and low-confidence ranges (dotted lines); see Supplementary Section S1 for discussion.

Table 1. Comparison of DNA thermodynamics measurement methods. Valid temperature range indicates a temperature span in which each method can directly measure ΔG° without extrapolation.

Method	ΔG° standard error	Valid temp. range	Throughput (# of ΔG° values)	DNA conc.
UV melting analysis	0.4 kcal/mol	Single	31 / plate	1 μM
High resolution melt	1.0 kcal/mol	Single	31 / plate	3 μM
Isothermal titration calorimetry (ITC) (17)	0.1 kcal/mol	Single	1 / cell	5000 μM
Differential scanning calorimetry (DSC)	>1.0 kcal/mol	Single	1 / cell	100 μM
Noncovalent catalysis (8)	0.1 kcal/mol	Single	20 / gel	0.6 μM
TEEM (this work)	0.05 kcal/mol	40+ °C	1200 / plate	1 μM

ΔG° 's change over temperature. These trends can otherwise be easily obscured by extrapolation.

In this paper, we first explain the basic principle of measuring ΔG° by TEEM and a general guideline for performing experiments. To help readers further improve the accuracy of their TEEM results, we also provide details on how to fine-tune reaction yields to minimize measurement errors. We then explain how to measure $\Delta\Delta G^\circ$ of a motif with TEEM and validate the method from multiple perspectives. By applying TEEM to a variety of destabilizing motifs common in biology and biotechnology, we report a novel discovery that $\Delta\Delta G^\circ$ of those motifs are mostly temperature-invariant.

MATERIALS AND METHODS

Materials

Phosphate buffer saline (PBS), Tris-EDTA (TE) buffer, and Tween 20 were purchased from Sigma-Aldrich. SYTO-13 intercalating dye was purchased from Life Technologies.

All oligonucleotides except those with N^6-methyladenine (6mA) and those for DSC were synthesized at the 100 nmol scale, and dissolved in TE buffer (pH 8.0) to 100 μM, and HPLC-purified by Integrated DNA Technologies (IDT). Chemical modifications on oligonucleotides were prepared by IDT as well. The majority of experiments performed utilize C oligonucleotides bearing a single ROX functionalization, except for a minor of C oligos bearing dual functionalization (ROX and FAM). All P oligonucleotides with single quencher had Iowa Black RQ to quench corresponding ROX, and the ones with double quencher had Iowa Black RQ and Iowa Black FQ to quench ROX and FAM, respectively. Oligonucleotides with 6mA were synthesized at the 1 μmol scale and purified by TriLink BioTechnologies. Oligonucleotides for DSC were synthesized at the 1 μmole scale and HPLC-purified by IDT.

The sequences of all oligonucleotides are listed in Supplementary Table S1. The concentrations of oligonucleotides stocks were verified with NanoDrop 2000 (Thermo Fisher), and then diluted to 10 μM in PBS. All DNA and RNA

oligonucleotides were stored in darkness at 4°C and −20°C, respectively.

Solution fluorescence for HRM and TEEM was measured using a QuantStudio 7 Flex instrument (Applied Biosystems). Samples were loaded in MicroAmp Fast Optical 96-Well Reaction Plates, 0.1 ml (Applied Biosystems), and the loaded plate was sealed using MicroAmp Optical Adhesive Film (Applied Biosystems).

Basics of TEEM

A toehold exchange reaction is a DNA strand displacement reaction in which two DNA oligonucleotides with similar sequences (X and P) compete in hybridization to a third oligonucleotide (16). Each X and P has a unique sequence that is complementary to the third oligonucleotide C to allow rapid strand displacement kinetics and equilibration; simultaneously, the toeholds are weak enough so that the binding of X and P to C are mutually exclusive.

In TEEM, the P oligo is functionalized with a quencher and the C oligo is functionalized with a fluorophore, so that solution fluorescence varies linearly with the concentration of the CX species. Figure 2A shows the three samples required for yield calculation: the toehold exchange reaction (Reaction), the minimum signal sample with C and P oligo but not X (Min), and the maximum signal sample with C and X oligo but not P (Max). The fluorescence of these samples is measured and normalized to calculate toehold exchange yields which are defined to be the equilibrium CX concentration divided by the total concentration of C in any state (Figure 2B). Note that C strands always form either CX or CP species because the strands are designed to have sufficiently high K_{eq}, which is also noted in our TEEM Oligonucleotides Sequence Design section (see also Figure 3) and the concentration of C is lower than the sum of those of X and P. This calculation holds because CP is low fluorescence and CX is high fluorescence, due to the colocalization and delocalization of the quencher (black square in Figure 2A). The solution fluorescence of a toehold exchange reaction comes from both CX and CP; if we define unit fluorescence $F_{CX} = R \cdot F_{CP}$, where R is the quenching ratio (typically around 50), then total fluorescence would be $F = F_{CX} \cdot [CX] + F_{CP} \cdot [CP] = F_{CP} \cdot ([C]_{total} + (R - 1) \cdot [CX])$. The Min sample represents quenched fluorescence when $[CX] = 0$, and the Max sample represents unquenched fluorescence when $[CX] = [C]_{total}$.

Observing the equilibrium fluorescence thus allows inference of the reaction equilibrium constant and ΔG° (Figure 2C). Importantly, because toehold exchange reactions equilibrate quickly, ramping the temperature of the reaction allows rapid and accurate acquisition of reaction ΔG° values for many different temperatures (Figure 2D, Supplementary Section S2).

TEEM can be used to infer the $\Delta\Delta G^\circ$ of motifs such as single-base bulges through numerical subtraction of experimental ΔG° values for two closely related reactions that differ by the motif of interest (Figure 2E and F). See Supplementary Section S3 for discussion on possible deviation between motif $\Delta\Delta G^\circ$ and the numerical difference between the two ΔG°_{rxn} values. To ensure TEEM method reproducibility, we typically performed nine replicates for each reaction ΔG° measurement; inferred ΔG° usually exhibited standard deviations of less than 0.04 kcal/mol at each temperature.

HRM

For HRM experiments, relevant duplex stock solutions were diluted to 3 μM in PBS with 0.1% (v/v) Tween 20, and then were serially diluted to 2, 1, 0.5, 0.3, 0.2 and 0.1 μM with the same buffer. Each sample was mixed with the same volume of 10 μM SYTO-13 dye in the same buffer. Samples were then transferred to wells in a 96-well plate, heated at the rate of 2°C/s until reaching 95°C, and denatured for 30 s. The plate was cooled down at the rate of −0.033°C/s until reaching 25°C, where it stayed for 10 min, and then melting started. Fluorescence was measured after increasing temperature by 0.1°C and holding for 5 seconds until reaching 95°C. The methods for analyzing HRM data are described in Supplementary Section S1.

TEEM oligonucleotides sequence design

Designing TEEM oligonucleotides is simpler than designing PCR primers. The first step is generating a sequence B where a motif of interest will be placed later (Figure 3). In our experience, sequences B with lengths of between 35 and 40 nucleotides and GC contents of between 40% and 60% work well, and having G at the first and the last positions of sequences B tends to result in better reaction yields. The C oligo has two toeholds attached to each side of the sequence B and a fluorophore at the 3′-end. Based on our studies of the effect of a toehold sequence on TEEM performance, we typically add TGGGTG to the 5′-side and ATATAT to the 3′-side of a sequence B. These toehold sequences work in most cases. If using the default toehold sequences is not feasible, it is possible to design new toeholds according to Supplementary Section S4. At this point, it is important to use DNA folding software such as NUPACK (4) to check and make sure the C oligo does not have any significant secondary structures which will disrupt toehold exchange equilibrium. We recommend redesigning the C oligo if NUPACK predicts free energy of strand (not to be confused with minimum free energy) more negative than −2.5 kcal/mol at 25°C and 0.15 M of sodium ion. The P oligo sequence design is straightforward; its sequence is complementary to the sequence B and the toehold on the 3′-side of the sequence B, and it has a quencher at the 5′-end. Designing the reference X oligo is very similar to designing the P oligo except that its sequence is complementary to the sequence B and the toehold on the 5′-side of the sequence B. When placing a destabilizing motif on a reference X oligo to create a Motif X oligo sequence, it is important to confirm that adding a motif sequence does not create any secondary structures.

Performing TEEM experiments

For TEEM experiments, relevant C and P stock solutions were diluted to 500 nM in PBS with 0.1% (v/v) Tween 20. Stocks of X oligos that formed only canonical base

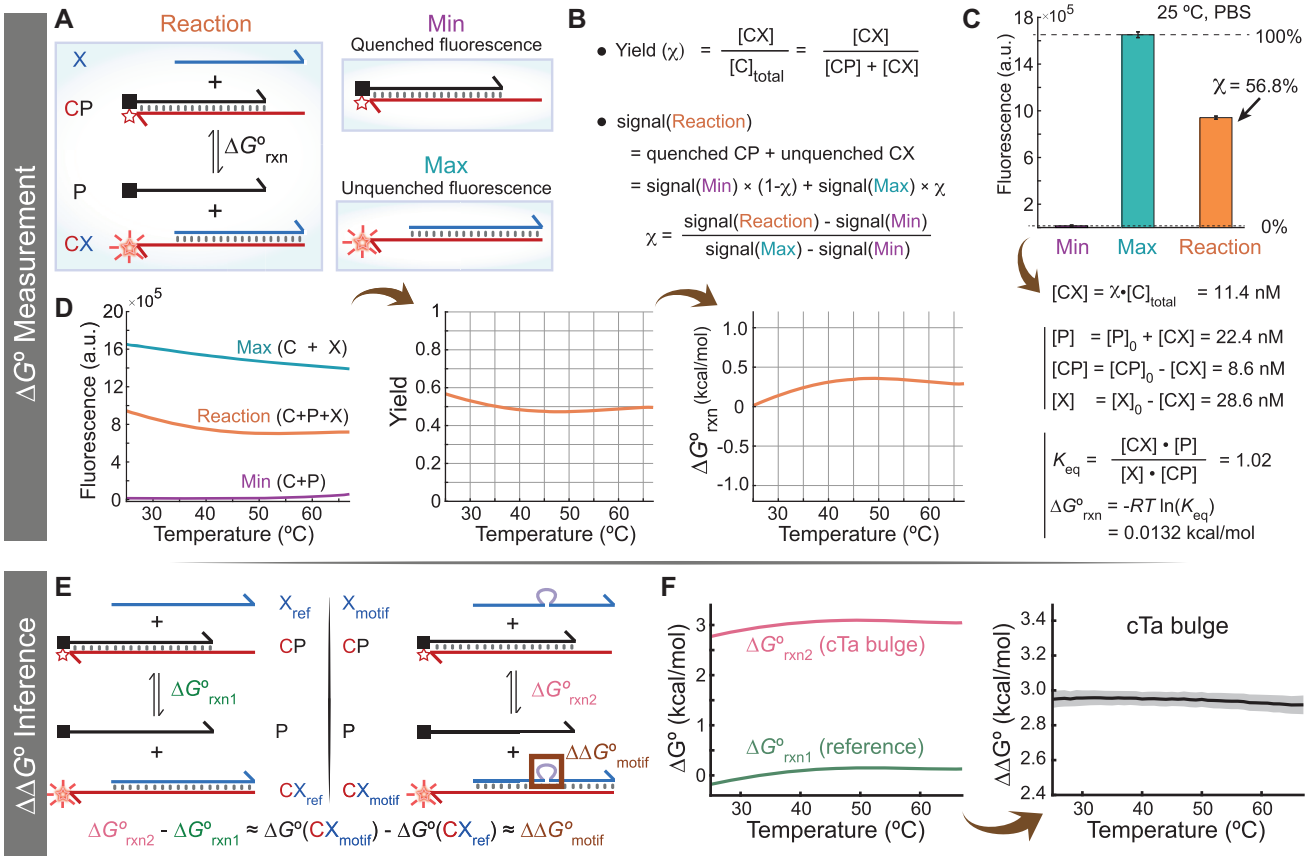

Figure 2. TEEM accurately measures the standard free energy (ΔG°_{rxn}) of a strand displacement reaction based on observed fluorescence (A-D) and infers a motif's $\Delta\Delta G^\circ$ by subtracting the ΔG°_{rxn} for two closely related reactions (EF). (**A**) Toehold exchange reactions (16) are DNA strand displacement reactions in which two DNA strands with similar sequence (X and P) compete in hybridization to a third strand (C). It rapidly equilibrates via hybridization to the single-stranded toehold regions of the duplex. Yield calculation requires 3 samples: the toehold exchange sample (Reaction), the minimum signal sample (Min), and the maximum signal sample (Max). (**B**) The yield of toehold exchange is defined as a ratio of CX duplex to total C oligo, and can be calculated based on the fluorescence intensities of the three samples. (**C**) Observed Min, Max, and Reaction fluorescence values for the strand displacement reaction. The yield χ is linearly interpolated to be 56.8%, and is used to calculate the equilibrium concentrations of CX, P, CP and X, which are then used to calculate the K_{eq} and ΔG°_{rxn}. Error bars show 1 standard deviation calculated based on 9 replicate experiments. (**D**) Experimental fluorescence values, inferred yields, and inferred ΔG°_{rxn} values for the same reaction at temperatures from 25°C to 67°C. (**E**) Two toehold exchange reactions are designed in a way that the difference in ΔG°_{rxn} values closely approximates the $\Delta\Delta G^\circ$ of the motif of interest (here, the brown bulge). (**F**) Inferred ΔG°_{rxn} values from fluorescence experiments, and corresponding inferred $\Delta\Delta G^\circ$ values for the cTa bulge. The shaded region around the $\Delta\Delta G^\circ$ trace denotes ±1 standard deviation, from 9 replicate experiments for each of reactions 1 and 2.

pairs with C oligos were diluted to 400 nM. Stocks of X oligos with a motif of interest were diluted to 15 μM (for 3-nt bulges), 10 μM (for single-nucleotide bulges, mismatches, and deamination), 1 μM (for phosphorothioate backbone) or 400 nM (for coaxial stack).

For the toehold exchange reactions, C and P oligos were mixed first and then X oligo was added afterwards, as illustrated in Figure 4A. Min and Max samples for characterizing minimum and maximum fluorescence signals were prepared by adding PBS in place of the X or P oligos, respectively. For higher throughput, testing multiple X oligos against a pair of C and P oligos is recommended to avoid having multiple Min and Max samples.

Reaching equilibration is important for accurate TEEM measurements of thermodynamics. To verify whether fluorescence measurements reflect equilibrium conditions, we measured fluorescence at every integer temperature between 20 and 70°C twice: when the solution was being gradually cooled, and when the solution was being gradually warmed. Consistency between the two measurement implies that equilibrium is established, while hysteresis would suggest that equilibrium has not been reached. Figure 4B shows the final time-temperature profile of our experiments and the points at which we performed fluorescence measurements (orange dots). This protocol was optimized for a balance of speed and accuracy: longer protocols with extended waiting time at each temperature would decrease the experimental throughput, and shorter protocols would result in the solution being far from equilibrium. Between the cooling and heating phase, temperature was maintained at 20°C for 1 h for another check to see whether equilibration was complete. The heating phase was the reverse of the cooling phase, and all temperature changes were performed at the rate of 2°C/s, after which the system waited for 4 or 7 min to allow equilibration. The median value of hysteresses calculated from all 4300 yields in 100 experiments was

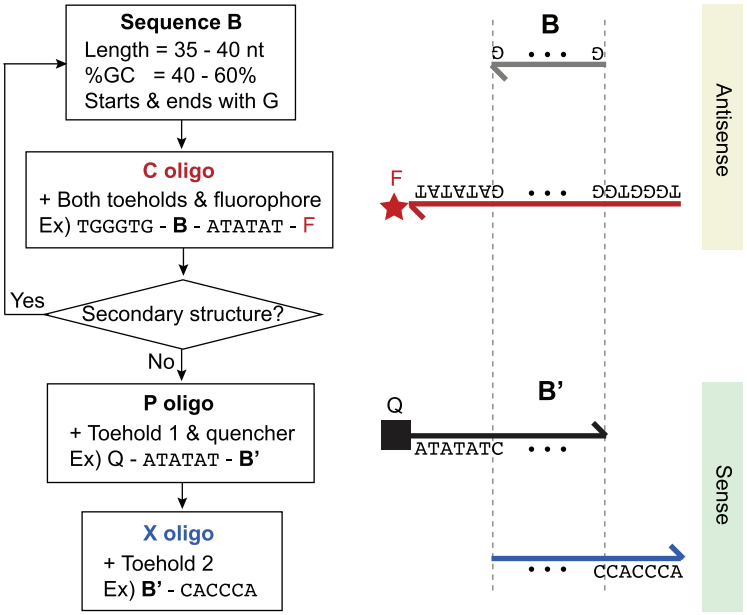

Figure 3. Workflow of designing TEEM oligo sequences. Start with designing a sequence B, where a motif of interest will be placed later. C oligo has two toeholds attached to each side of sequence B and a fluorophore at the 3′-end. Here, we show our default toehold sequences that work well in most cases, but we also have a guideline for designing a customized toehold sequence (Supplementary Section S4). After checking whether C oligo has any secondary structures, P oligo can be designed with a sequence complementary to sequence B and the toehold on the 3′-side of sequence B, with a quencher attached at the 5′-end. The sequence of X oligo is complementary to sequence B and the toehold on 5′-side of sequence B.

0.0019, which indicated that hysteresis of TEEM was negligibly small (Supplementary Section S2).

Differential scanning calorimetry

DSC was performed using a DSC 250 instrument (TA Instruments). Oligonucleotides were first dissolved in PBS with 0.1% (v/v) Tween 20 to 500 μM, and their concentrations were measured with NanoDrop. Next, the relevant oligos were mixed to create 100 μM duplex. Sample solutions were pre-annealed by heating at 95°C for 3 min and cooling down to 25°C at the rate of −1°C per 10 sec. Sample and buffer solutions were then degassed by ultrasonication for 10 min using Bransonic 1800 (Branson). Twenty microliters of each solution were placed in a Tzero aluminium pan and covered with a Tzero aluminium hermatic lid (TA Instruments). Starting from incubating at 40°C for 5 min, the samples were heated to 110°C at the rate of 5°C/min during DSC.

RESULTS

HRM measurements of single-base bulges

At high temperatures, the entropic loss of forming double-stranded DNA (dsDNA) overcomes the enthalpic gain, so DNA becomes single-stranded. DNA duplexes of different stabilities have different T_m. T_m also changes based on DNA concentrations. In HRM experiments, a fluorescent dye specifically intercalates dsDNA, and produces lower fluorescence when not intercalated. Analysis of the temperature-based change in solution fluorescence produces estimates of the ΔH° and ΔS° of DNA duplex formation by assuming they are temperature-invariant (Supplementary Section S1). For our experiments, we used SYTO-13 as the intercalating dye (18–20) because the literature and our experience indicate that this dye has minimal impact on DNA binding thermodynamics.

When HRM is applied to two closely related DNA sequences that differ by a single bulge (Figure 1B), the differences in the two fitted ΔH° and ΔS° values can be considered to be the $\Delta\Delta H^\circ$ and $\Delta\Delta S^\circ$ of the bulge, which then can be used to calculate the motif $\Delta\Delta G^\circ$ at different temperatures T via $\Delta\Delta G^\circ = \Delta\Delta H^\circ - T \cdot \Delta\Delta S^\circ$. We performed pairs of HRM experiments on four different DNA duplexes and their corresponding single-base bulge variations (Figure 1C). The four duplexes were designed to be of different lengths and thus had different T_m values, but the single-base bulge was conserved to be a T flanked by a C to the 5′ end and an A to the 3′ end (henceforth cTa bulge). The four experiments on the cTa bulge should give the same $\Delta\Delta G^\circ$ values based on the NN model of DNA thermodynamics, but were observed experimentally that they produced mutually incompatible results with variations of up to 3 kcal/mol. This implied either that the NN model of DNA thermodynamics was incorrect or that the HRM method for measuring DNA thermodynamics was inaccurate.

Verifying fluorescence measurement

To validate the basis of TEEM, we verified the quality of raw fluorescence data from which TEEM inferred the yields of hybridization reactions (Supplementary Section S2). In the concentration regime that we experimentally worked with, we observed near-perfect linear relationship between fluorescence and the concentration of an oligo with ROX (Supplementary Figure S2-1a). There was no light spillover

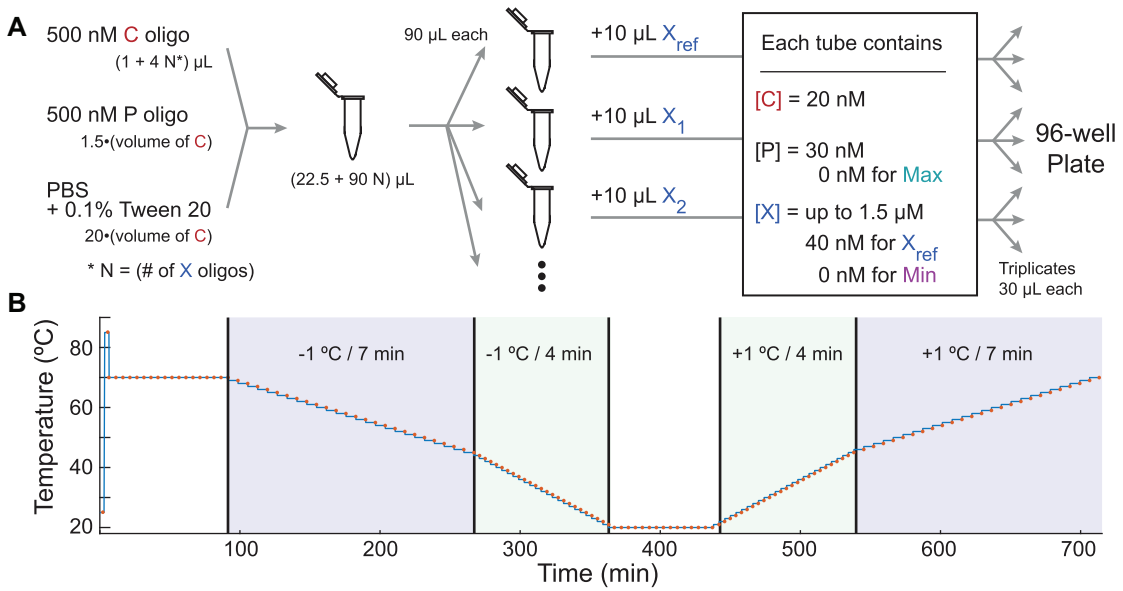

Figure 4. Experimental procedure of TEEM. (**A**) Protocol for preparing samples of TEEM fluorescence analysis. First, create a mixture of C and P oligos. Divide them into 90 µL based on the number of X oligos, and add 10 µl of each X oligo. For fluorescence measurement, divide each sample into three 30 µl as triplicates, and transfer them to a qPCR plate. For Min or Max samples, add the buffer instead of X or P oligo, respectively. (**B**) Temperature program of TEEM. Orange dots indicate where fluorescence signals are measured. After the initial denaturation at 85°C for 3 min, temperature stays at 70°C for 1.5 h with measurements every 5 min to confirm that equilibrium has been reached before cooling starts. From 70°C to 45°C, 7 min of waiting follows every −1°C change, and fluorescence is measured at the end of each waiting time. Equilibration was observed to be faster at lower temperatures, so from 44°C to 20°C, only 4 min of waiting time is applied per −1°C change.

observed among wells with reaction solutions, suggesting that the measured fluorescence accurately reflected only the sample of interest and was not affected by neighboring wells (Supplementary Figure S2-1a). We also confirmed that photobleaching of ROX at various temperatures was negligible (Supplementary Figure S2-1b). When using a fluorescence plate reader without any uniformity calibration function, it is important to manually normalize fluorescence intensities to correct position-based bias. The normalization factor can be easily calculated by measuring the intensities of a plate filled with the same ROX solution and dividing each intensity by the highest one (Supplementary Figure S2-2).

Reaction ΔG° range for accurate TEEM analysis

TEEM calculates $\Delta G^\circ_{\text{rxn}}$ from toehold exchange reaction yield. Insofar as solution fluorescent measurement has non-zero noise, errors in fluorescence measurement propagate to errors in yield and $\Delta G^\circ_{\text{rxn}}$. Mathematically, for a toehold exchange reaction with yield $\chi = y/[\text{C}]_{\text{total}}$ (where y is the concentration of CX formed):

$$\Delta G^\circ_{\text{rxn}} = -RT\ln K_{eq} = -RT\ln\frac{y([\text{P}]_0 + y)}{([\text{CP}]_0 - y)([\text{X}]_0 - y)} \quad (1)$$

Here, R is the gas constant, T is temperature, and $[\text{P}]_0$, $[\text{CP}]_0$ and $[\text{X}]_0$ are the initial concentrations of each species. Assuming Gaussian-distributed noise in fluorescence and inferred χ, the error in $\Delta G^\circ_{\text{rxn}}$ values is larger when χ is at extremal values near 0 or 1. This can be simply understood as the partial derivative of yield with respect to ΔG° being maximized when χ is around 0.5, because $\Delta(\Delta G^\circ) \approx \frac{\partial \Delta G^\circ}{\partial \chi} \cdot \Delta\chi$. For a constant yield measurement error $\Delta\chi$, the propagated error in standard free energy $\Delta(\Delta G^\circ)$ grows as $\frac{\partial \Delta G^\circ}{\partial \chi}$ becomes larger, or $\frac{\partial \chi}{\partial \Delta G^\circ}$ becomes smaller. Figure 5B shows the analytic relationship between χ and ΔG°, and Figure 5C plots the partial derivative $\frac{\partial \chi}{\partial \Delta G^\circ}$ against ΔG°. Plotted in Figure 5B and C are the lines corresponding to yields χ wherein the ΔG° inference has 2.5× and 5× larger error than the minimum error achieved at $\chi = 0.5$. For all 4300 TEEM measurements included in this paper, all observed yields were within the range of 4.5% to 95.7% range (Figure 5A).

Yield tuning with P and X oligonucleotides

For a given set of concentrations $[\text{P}]_0$ and $[\text{X}]_0$, the ΔG° at which $\chi = 0.5$ is fixed: For example, if $[\text{P}]_0 = [\text{X}]_0$, then $\chi = 0.5$ when $\Delta G^\circ = 0$, and the range of ΔG° values that can be accurately measured is approximately from –2 kcal/mol to +2 kcal/mol. However, the accurate range of ΔG° inference can be adjusted based on the relative concentrations of $[\text{P}]_0$ and $[\text{X}]_0$. Figure 5D illustrates the tuning: When the initial concentration of P increases 10-fold, the acceptable ΔG° range shifts from –2 to +2 kcal/mol to –4 to 0 kcal/mol. If instead the initial concentration of X oligo is increased 25-fold, then the acceptable ΔG° range shifts to +0.5 to +4.5 kcal/mol. We confirmed that experimental yields of TEEM could be tuned by increasing the initial concentration of X oligo (Figure 5E and F). Therefore, it is possible that we can greatly expand the range of ΔG° values that we can accurately infer by increasing $[\text{P}]_0$ or $[\text{X}]_0$ up to 1000-fold over $[\text{C}]_0$.

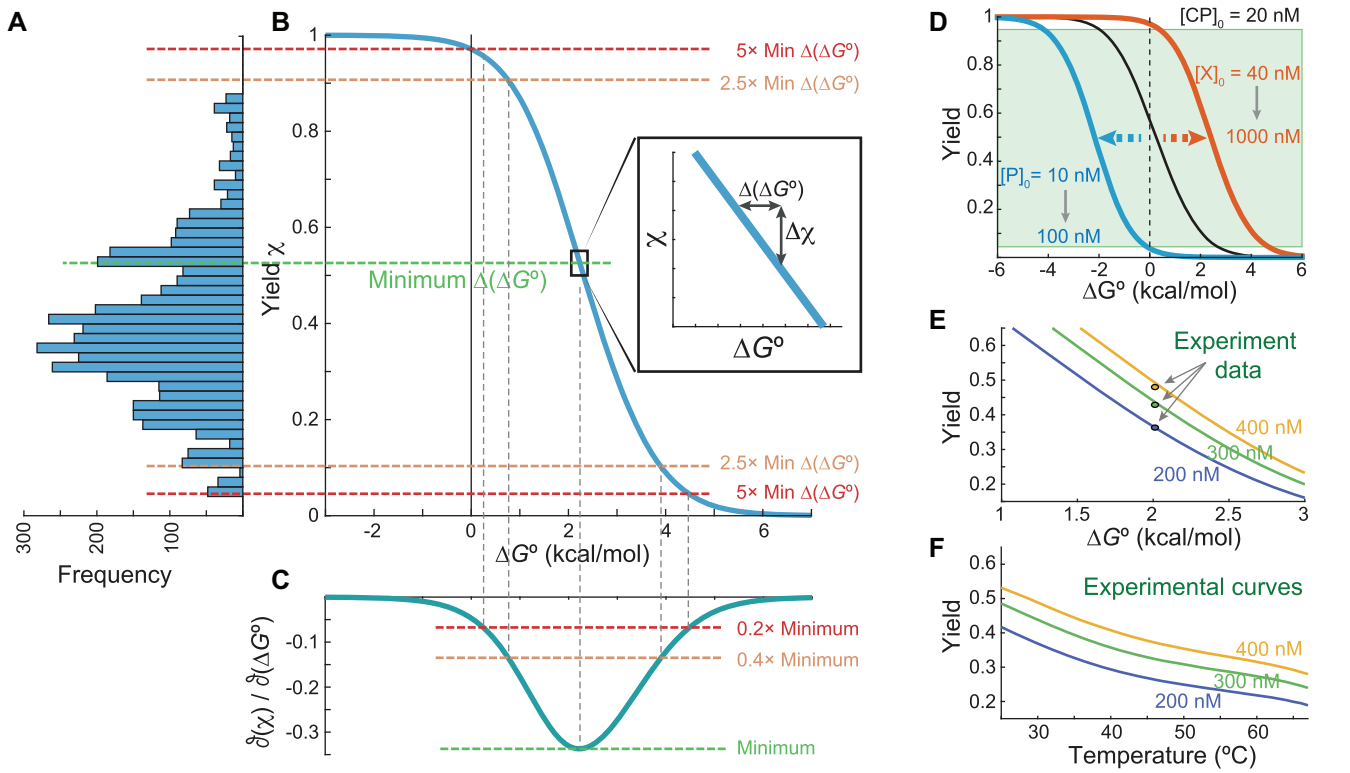

Figure 5. Reaction yields can be fine-tuned to minimize TEEM measurement standard error. (**A**) The histogram summarizes the 4300 observed experimental reaction yields measured in this work, from 100 experiments across temperatures from 25°C to 67°C. (**B**) Relationship between hybridization yield χ and reaction standard free energy ΔG°, at the experimental concentrations of $[CP]_0 = 20$ nM and $[P]_0 = 10$ nM. Assuming that the measurement error on yield χ is a constant numerical amount, the ΔG° inference error is minimized where the slope is steepest at $\chi \approx 50\%$. At yields of $\chi \approx 5\%$ and $\chi \approx 95\%$, the ΔG° inference error is 5 times higher than the minimal error, and we consider the range of yield between 5% and 95% to be our acceptable quantitation range. (**C**) The derivative of the reaction yield vs. the reaction standard free energy ΔG° at different values of ΔG°. The inference error of ΔG° based on errors in χ value is inversely proportional to the plotted value. (**D**) The range of measurable ΔG° can be tuned by controlling the initial concentrations of P and X. The green shaded region indicates the acceptable yield range where ΔG° inference error is less than 5× minimum error. Default concentrations (black text) creates steepest slope around $\Delta G^\circ = 0$ kcal/mol (black line), with an acceptable range of ΔG° from –2 kcal/mol to +2 kcal/mol. If $[P]_0$ is increased, the whole plot shifts left (blue plot) and more negative ΔG° can be measured reliably. If $[X]_0$ is increased, the whole plot shifts right (orange plot) and more positive ΔG° can be measured. (**E**) Experimental demonstration of tuning at a single temperature. As $[X]_0$ is increased from 200 nM to 400 nM, yield also increases according to theoretical plot. (**F**) Experimental demonstration of tuning across different temperature. Higher $[X]_0$ results in higher yields at all temperatures, consistent with expectations.

Measuring motif thermodynamics with TEEM

Our TEEM results on the cTa bulge show $\Delta\Delta G^\circ$ values of roughly 3.0 kcal/mol across temperatures from 25°C to 67°C. These results were actually consistent with HRM results for each of the four sequences when considering only the HRM results at temperatures near T_m, where HRM ΔG° inference was most accurate (Figure 6A). Our results thus suggested that ΔG° inferred from HRM data did not extrapolate well to broad temperature ranges.

To verify the accuracy of TEEM measurements of motif $\Delta\Delta G^\circ$ values, we designed TEEM reactions to measure the thermodynamics of base stacks. Unlike bulges and mismatches, base stacks have been characterized rigorously and systematically by many groups (26–28) with various T_m, so reported base stack thermodynamics are unlikely to contain significant error. We measured the ΔG° of the 5′-TC-3′ and 5′-CC-3′ base stacks for three different DNA sequences each, and the TEEM ΔG° values were highly consistent both with each other and with literature values (Figure 6B). See Supplementary Section S5 for further details on base stack ΔG° measurement.

To further verify that the NN model was an accurate approximation of true DNA thermodynamics, we next designed three additional sets of DNA oligos to test whether the same aCc bulge motif exhibited similar $\Delta\Delta G^\circ$ values when presented at different positions in different DNA duplexes (Figure 6C, Supplementary Section S5). All three sets of experiments on the aCc bulge produced $\Delta\Delta G^\circ$ values within 0.1 kcal/mol of each other for all temperatures measured, supporting the NN model.

We next used TEEM to measure the $\Delta\Delta G^\circ$ of a variety of commonly observed or used DNA motifs (Figure 7 and Supplementary Section S6). Across the wide range of different structural and chemical motifs characterized, almost all $\Delta\Delta G^\circ$ values were quite temperature-invariant. Because other DNA thermodynamics characterization methods including HRM and DSC (Supplementary Section S8) can only acquire thermodynamics parameters at a single temperature and have large standard errors, this phenomenon has not been previously observed.

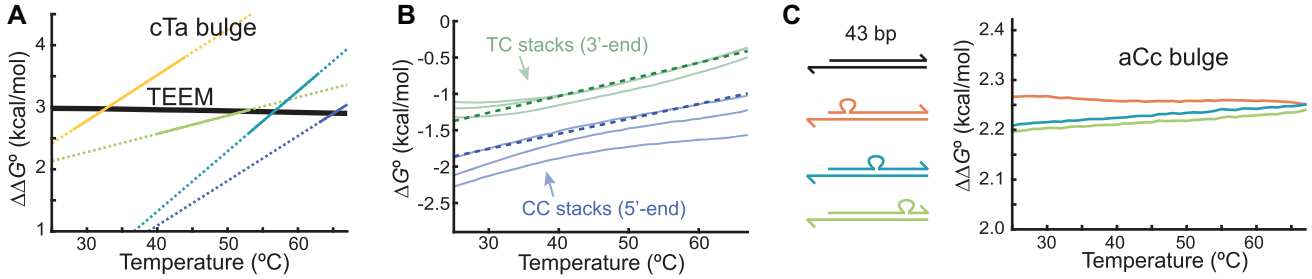

Figure 6. Validating TEEM from three different perspectives. (**A**) Comparison of the cTa bulge $\Delta\Delta G^\circ$ values measured by TEEM versus by HRM. Colored lines show HRM results on different duplexes. The TEEM $\Delta\Delta G^\circ$ values are consistent with all four HRM measurements in their high-confidence ranges (solid lines). (**B**) TEEM characterization of TC base stacks and CC base stacks, each for 3 different duplexes. For each type of base stack, the inferred ΔG° values are consistent with each other, and also consistent with previously literature-reported values (dotted lines, from (10)). See Supplementary Section S5 for schematic. (**C**) TEEM characterization of the aCc bulge motif at three different positions on three different DNA duplexes. All three measurements produced $\Delta\Delta G^\circ$ values within 0.1 kcal/mol of each other, supporting the NN model of DNA hybridization kinetics.

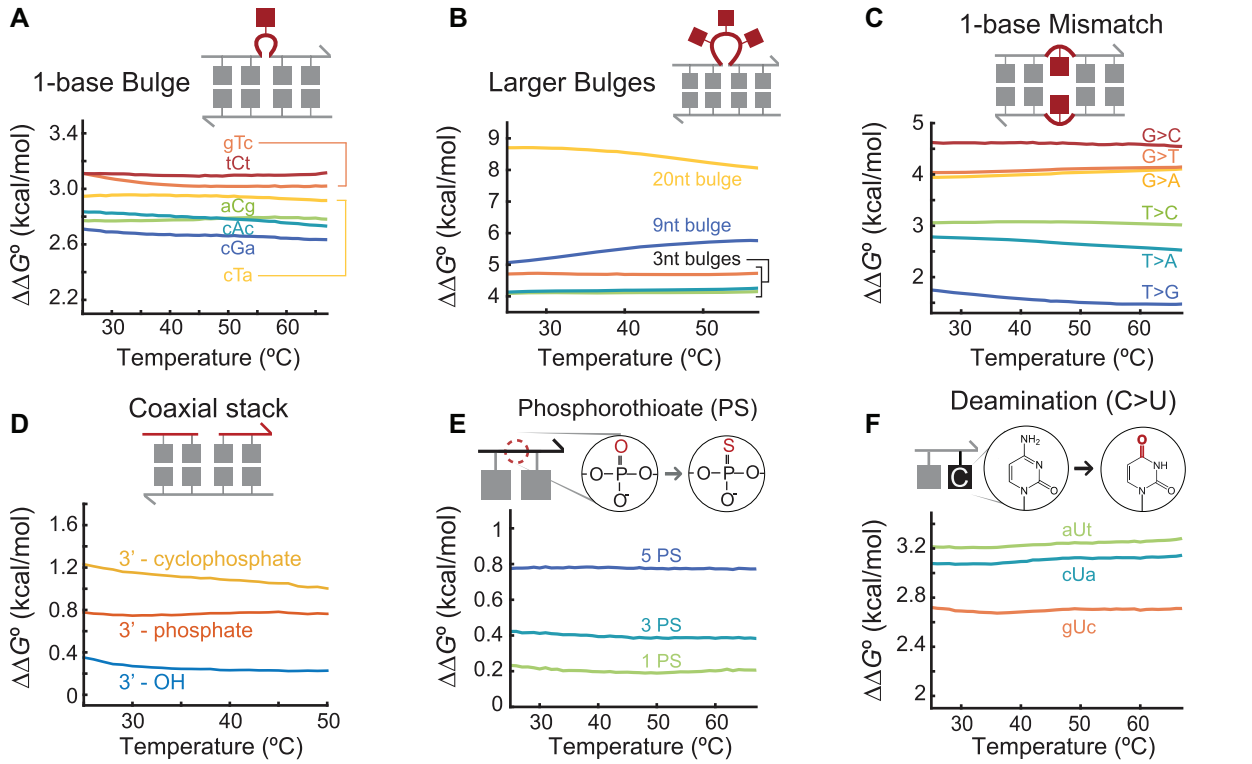

Figure 7. TEEM-measured $\Delta\Delta G^\circ$ values for several different types of DNA motifs; see Section S6 for more data. (**A**) Single-base bulges; occur biologically following DNA polymerase insertion/deletion events (21), and in biotechnology when synthetic oligonucleotides bear synthesis deletions (22). (**B**) Multi-base bulges; a two-step TEEM method was used for multi-base bulges, because of the larger associated $\Delta\Delta G^\circ$ values (Supplementary Section S7). (**C**) Single-base mismatches; occur biologically upon DNA polymerase nucleotide misincorporation (23), and in genomics when probes bind to single nucleotide polymorphisms or mutants. (**D**) Co-axial stacks; occur biologically and in biotechnology upon DNA nicking due to enzymatic activity (e.g. to repair damaged DNA) (Supplementary Section S7). (**E**) Phosphorothioate backbone modification; used in biotechnology to reduce nuclease susceptibility of synthetic oligonucleotides (24). (**F**) Deamination; occurs in aged formalin-fixed paraffin-embedded (FFPE) tissue samples (25).

DISCUSSION

Our TEEM method for thermodynamic characterization of DNA motifs has significantly higher throughput than all previous methods, and simultaneously is more precise. In addition, TEEM is generalizable to other nucleic acids such as RNA (Supplementary Section S9). These improved capabilities allowed us to accurately measure the $\Delta\Delta G^\circ$ of DNA motifs across a wide temperature range, which led us to discover that previously reported ΔH° and ΔS° were inaccurately extrapolated from DNA melt experiments. To support the validity of TEEM, we rigorously verified our new method (via a series of measurements of the same DNA motif in different contexts) and systematically replicated all of our motif thermodynamics experiments to minimize statistical error with at least nine replicate experiments for each motif. Based on our results, we are confident that the data we collected are indeed reflective of natural biophysics.

The accuracy of TEEM results relies upon the assumption that the motif $\Delta\Delta G^\circ$ can be approximated as the dif-

ference of reaction ΔG° values, which holds true when the single-stranded reference and variant DNA sequences exhibit similar folding energies. Insofar as DNA folding software relies on imperfect thermodynamic parameters, our measured $\Delta\Delta G^\circ$ values for any particular set of sequences may differ from objectively true values by a small amount. However, this systematic bias of ΔG° difference should not be temperature-dependent, so our observation regarding the temperature invariance of $\Delta\Delta G^\circ$ for DNA destabilization motifs should hold. Furthermore, our experiments on several independent DNA sequences with the same motif (Figure 6C, Supplementary Figure S5-1) showed variation of less than 0.1 kcal/mol, indicating that any error if present is likely small.

One limitation of the TEEM method is that it cannot be used to directly measure large values of $\Delta\Delta G^\circ >$ 4 kcal/mol, because hybridization yields will be saturated to close to 0 or 1, resulting in larger inference errors. In Figure 7B (larger bulges) and Supplementary Section S7, we show that multi-step TEEM can be used to measure motifs with large $\Delta\Delta G^\circ$ values. However, multi-step TEEM will have increased errors compared to single-step TEEM due to error propagation.

DATA AVAILABILITY

All experimental data are plotted in the Supplementary Materials, and numerical data files are available upon request.

SUPPLEMENTARY DATA

Supplementary Data are available at NAR Online.

ACKNOWLEDGEMENTS

The authors thank Jianyi Nie for editorial assistance.
Author contributions: J.B. conceived the project, designed and conducted the experiments, analyzed the data and wrote the paper. D.Y.Z. conceived the project, analyzed the data and wrote the paper.

FUNDING

National Human Genome Research Institute [R01HG008752 to D.Y.Z.]. Funding for open access charge: National Human Genome Research Institute [R01HG008752].
Conflict of interest statement. D.Y.Z. is a co-founder and significant equity holder of NuProbe Global and of Torus Biosystems, and is a consultant for Avenge Bio.

REFERENCES

1. Schirle,N.T., Sheu-Gruttadauria,J. and MacRae,I.J., (2014) Structural basis for microRNA targeting. *Science*, **346**, 608–613.
2. Zhang,J.X., Fang,J.Z., Duan,W., Wu,L.R., Zhang,A.W., Dalchau,N. and Zhang,D.Y., (2018) Predicting DNA hybridization kinetics from sequence. *Nat. Chem.*, **10**, 91.
3. Zuker,M., (2003) Mfold web server for nucleic acid folding and hybridization prediction. *Nucleic Acids Res.*, **31**, 3406–3415.
4. Zadeh,J.N., Steenberg,C.D., Bois,J.S., Wolfe,B.R., Pierce,M.B., Khan,A.R. and Pierce,N.A., (2011) NUPACK: analysis and design of nucleic acid systems. *J. Comput. Chem*, **32**, 170–173.
5. Freier,S.M., Kierzek,R., Jaeger,J.A., Sugimoto,N., Caruthers,M.H., Neilson,T. and Turner,D.H., (1986) Improved free-energy parameters for predictions of RNA duplex stability. *Proc. Natl. Acad. Sci. U.S.A.*, **83**, 9373–9377.
6. SantaLucia,J., (1998) A unified view of polymer, dumbbell, and oligonucleotide DNA nearest-neighbor thermodynamics. *Proc. Natl. Acad. Sci. U.S.A.*, **95**, 1460–1465.
7. Dirks,R.M., Bois,J.S., Schaeffer,J.M., Winfree,E. and Pierce,N.A., (2007) Thermodynamic analysis of interacting nucleic acid strands. *SIAM Rev.*, **49**, 65–88.
8. Wang,C., Bae,J.H. and Zhang,D.Y., (2016) Native characterization of nucleic acid motif thermodynamics via non-covalent catalysis. *Nat. Commun.*, **7**, 10319.
9. Tinoco,I., Uhlenbeck,O.C. and Levine,M.D., (1971) Estimation of secondary structure in ribonucleic acids. *Nature*, **230**, 362–367.
10. SantaLucia,J. Jr. and Hicks,D., (2004) The thermodynamics of DNA structural motifs. *Annu. Rev. Biophys. Biomol. Struct.*, **33**, 415–440.
11. Jackson,A.L. and Loeb,L.A., (2001) The contribution of endogenous sources of DNA damage to the multiple mutations in cancer. *Mutat. Res./Fundam. Mol. Mech. Mutagen.*, **477**, 7–21.
12. Buermeyer,A.B., Deschenes,S.M., Baker,S.M. and Liskay,R.M., (1999) Mammalian DNA mismatch repair. *Annu. Rev. Genet.*, **33**, 533–564.
13. Richter,C., Park,J.W. and Ames,B.N., (1988) Normal oxidative damage to mitochondrial and nuclear DNA is extensive. *Proc. Natl. Acad. Sci. U.S.A.*, **85**, 6465–6467.
14. da Silva,J., (2016) DNA damage induced by occupational and environmental exposure to miscellaneous chemicals. *Mutat. Res./Rev. Mutat. Res.*, **770**, 170–182.
15. Wittwer,C.T., (2009) High-resolution DNA melting analysis: advancements and limitations. *Hum. Mutat.*, **30**, 857–859.
16. Zhang,D.Y., Chen,S.X. and Yin,P., (2012) Optimizing the specificity of nucleic acid hybridization. *Nat. Chem.*, **4**, 208–214.
17. Vaitiekunas,P., Crane-Robinson,C. and Privalov,P.L., (2015) The energetic basis of the DNA double helix: a combined microcalorimetric approach. *Nucleic Acids Res.*, **43**, 8577–8589.
18. Gudnason,H., Dufva,M., Bang,D.D. and Wolff,A., (2007) Comparison of multiple DNA dyes for real-time PCR: effects of dye concentration and sequence composition on DNA amplification and melting temperature. *Nucleic Acids Res.*, **35**, e127.
19. Eischeid,A.C., (2011) SYTO dyes and EvaGreen outperform SYBR Green in real-time PCR. *BMC Research Notes*, **4**, 263.
20. Radvanszky,J., Surovy,M., Nagyova,E., Minarik,G. and Kadasi,L., (2015) Comparison of different DNA binding fluorescent dyes for applications of high-resolution melting analysis. *Clin. Biochem.*, **48**, 609–616.
21. Mills,R.E., Luttig,C.T., Larkins,C.E., Beauchamp,A., Tsui,C., Pittard,W.S. and Devine,S.E., (2006) An initial map of insertion and deletion (INDEL) variation in the human genome. *Genome Res.*, **16**, 1182–1190.
22. Kosuri,S. and Church,G.M., (2014) Large-scale de novo DNA synthesis: technologies and applications. *Nat. Methods*, **11**, 499–507.
23. Potapov,V. and Ong,J.L., (2017) Examining sources of error in PCR by single-molecule sequencing. *PloS one*, **12**, e0169774.
24. Skerra,A., (1992) Phosphorothioate primers improve the amplification of DNA sequences by DNA polymerases with proofreading activity. *Nucleic Acids Res.*, **20**, 3551–3554.
25. Kim,S., Park,C., Ji,Y., Kim,D.G., Bae,H., van Vrancken,M. and Kim,K.M., (2017) Deamination effects in formalin-fixed, paraffin-embedded tissue samples in the era of precision medicine. *J. Mol. Diagn.*, **19**, 137–146.
26. Owczarzy,R., Vallone,P.M., Gallo,F.J., Paner,T.M., Lane,M.J. and Benight,A.S., (1997) Predicting sequence-dependent melting stability of short duplex DNA oligomers. *Biopolymers*, **44**, 217–239.
27. Gotoh,O. and Tagashira,Y., (1981) Stabilities of nearest-neighbor doublets in double-helical DNA determined by fitting calculated melting profiles to observed profiles. *Biopolymers*, **20**, 1033–1042.
28. Breslauer,K.J., Frank,R., Blöcker,H. and Marky,L.A., (1986) Predicting DNA duplex stability from the base sequence. *Proc. Natl. Acad. Sci. U.S.A.*, **83**, 3746–3750.